Research Paper
Computational Methods for Differential Equations
http://cmde.tabrizu.ac.ir
Vol. 13, No. 4, 2025, pp. 1162-1176
DOI:10.22034/cmde.2024.59745.2547

Numerical multiscale methods to determine the coefficient in diffusion problems

Marzieh Tavakolian[1], **Ali Hatam**[1,*], **Morteza Fotouhi**[2], **and Edmund Chadwick**[3]

[1]Department of Applied Mathematics, Amirkabir University of Technology, No. 350, Hafez Ave, Valiasr Square, Tehran, Iran 1591634311.

[2]Department of Mathematical Sciences, Sharif University of Technology, Tehran 11365-9415, Iran.

[3]School of Computing, Science and Engineering, University of Salford, Salford, M5 4WT, UK.

Abstract

Here we study the inverse problem of determining the highly oscillatory coefficient a^ε in some PDEs of the form $u_t^\varepsilon - \nabla.(a^\varepsilon(x)\nabla u^\varepsilon) = 0$, in a bounded domain $\Omega \subset \mathbb{R}^d$; ε indicates the smallest characteristic wavelength in the problem $(0 < \varepsilon \ll 1)$. Assume that $g(t,x)$ is given input data for $(t,x) \in (0,T) \times \partial\Omega$ and the associated output is the thermal flux $a^\varepsilon(x)\nabla u(T_0,x) \cdot n(x)$ measured on the boundary at a given time T_0. Due to the ill-posedness of the inverse problem, we reduce the dimension by seeking effective parameters. For the forward solver, we apply either analytic homogenization or some numerical multiscale methods such as the FE-HMM and LOD method.

Keywords. Heterogeneous multiscale method, Homogenization, Inverse problem, Localized orthogonal decomposition method, Parabolic partial differential equations.

2010 Mathematics Subject Classification. 35B27, 35K20, 35R30, 65L60, 65M32.

1. Introduction

Many applications in engineering and technology, such as heat conduction, geoscience and wave scattering, biology, medical image processing, and so on, necessitate solving inverse problems for partial differential equations [10, 15]. This overview aims is to represent how multiscale modeling plays an essential role in solving inverse problems for differential equations. Here, we are going to determine the unknown parameters by matching observed data. Due to the multiscale structure, the forward problem involves more difficulties, such as high-level resolution in numerical computations. Hence, the inverse problem is further complicated. We are interested in PDEs that vary on a very fine scale, as a result of heterogeneity in the medium, for example.

Assume that the microstructure's nature is known, but it contains an unknown parameter. In this work, the inverse problem of determining the coefficient $a^\varepsilon(x)$ in the following model (1.1) has been investigated, where the superscript ε denotes the problem's multiscale nature (characteristic wavelength) and it is the ratio of scales in the model $(0 < \varepsilon \ll 1)$.

$$\begin{aligned} u_t^\varepsilon - \nabla \cdot (a^\varepsilon(x)\nabla u^\varepsilon) &= f(t,x), \quad \text{in } (0,T) \times \Omega, \\ u^\varepsilon(0,x) &= u_0(x), \quad \text{in } \Omega, \\ u^\varepsilon(t,x) &= g(t,x), \quad \text{on } (0,T) \times \partial\Omega, \end{aligned} \tag{1.1}$$

where $\Omega \subset \mathbb{R}^d$ is a bounded, open and connected domain with sufficiently smooth boundary $\partial\Omega$ and $a^\varepsilon(x) = a(x, x/\varepsilon) = (a_{il}(x, x/\varepsilon))_{1\le i,l\le d}$ is a symmetric $d \times d$ matrix valued function in Ω, satisfying the following conditions:

i) $a(x,y)$ is Y-periodic in y, where $Y = [0,1]^d$.
ii) $a(x,y)$ is bounded and uniformly elliptic i.e.,

$$a^\varepsilon(x)\xi \cdot \xi \ge \alpha|\xi|^2, \quad |a^\varepsilon(x)\xi| \le \beta|\xi|, \quad \text{for some } \alpha, \beta > 0. \tag{1.2}$$

Received: 24 December 2023 ; Accepted: 23 December 2024.
∗ Corresponding author. Email: alihatam@aut.ac.ir.

In this study, we measure the boundary value (thermal flux) $a^\varepsilon \nabla u(T_0)\cdot n_{|\partial\Omega}$ at a given fixed time $T_0 \in (0,T]$ for the problem (1.1), with assigning the temperature $g(t,x)$ on $\partial\Omega$. Associated input-output map is introduced as the operator

$$\Lambda_{a^\varepsilon} : g \mapsto a^\varepsilon \nabla u(T_0)\cdot n_{|\partial\Omega}. \tag{1.3}$$

We use the information from measurements from this map to look for the unknown parameter of this fine-scale structure. In [13], the authors have studied the inverse problem and shown the uniqueness of a^ε when Λ_{a^ε} is given.

Usually in standard approaches to such problems, solving the forward problem requires that the meshes be refined as possible to the smallest scale [5].

Solving such high-dimensional problems repeatedly provides a difficult computing challenge that is rarely tractable. The above multiscale parabolic problem (1.1) is an example showing these difficulties.

In this work, we use the prior assumption of a microscale parametrization $m \to a^\varepsilon(m,\cdot)$, where the parameter m belongs to an interval $[r,s]$.

Then the form of the coefficient a^ε becomes as follows

$$a^\varepsilon(m,x) = a(m,x,x/\varepsilon)I_d, \tag{1.4}$$

where the I_d denotes the $d\times d$ identity matrix. The function $a(m,x,x/\varepsilon)$ is assumed to be known, and the purpose is to find the unknown parameter m in the microstructure model of diffusion coefficient through some numerical multiscale methods.

This kind of multiscale inverse problem was originally introduced by C. Frederick and B. Engquist [18], for elliptic equations. They used numerical homogenization for a class of this problem and also made a connection with the theoretical results. In the present work, we have applied this theory to parabolic equations and also developed it for a wider range of diffusion coefficients. In 2019, A. Abdulle and A. Di Blasio analyzed recovering the whole tensor of the elliptic multiscale inverse problems in a class of parameterized anisotropic locally periodic multiscale tensors, $a^\varepsilon_\sigma(x) = a(\sigma(x),x/\varepsilon)$, when the function σ is unknown while the map $(\sigma,y)\mapsto a(\sigma,y)$ is assumed to be known [5]. Also in 2020, they considered the Bayesian numerical homogenization method for elliptic multiscale inverse problems [4].

The outline of this work is as follows. In section 2, we briefly describe the homogenization theory and how to evaluate the efficient coefficients. We also describe how the inverse problem has been, modeled and we address the uniqueness of the solution of the inverse problem. In section 3, the Finite Element Heterogeneous Multiscale Method (HMM) has been explained, and in section 4, we introduce the localized orthogonal decomposition method (LOD), also the convergence of the method as a forward solver has been shown in Figure 4. Both these methods can be applied when the explicit form of the homogenized coefficient is not available.

It should be mentioned that the approach of HMM emerged from analytical homogenization theory, and the analysis of this method is based on analytical homogenization and therefore requires some assumptions on the coefficient, such as scale separation or periodicity, and this is a difference between the LOD method and HMM [21, 24]. In section 5, some examples and numerical results regarding the parameter identification have been provided. Eventually, some results are shown in section 6.

2. Multiscale inverse problem

2.1. **Homogenized forward model.** In classical homogenization theory [11, 14], a positive definite matrix A is said to be the homogenized matrix for $a^\varepsilon(x) = a(x,x/\varepsilon)$, if for any bounded domain $\Omega\subset\mathbb{R}^d$ with C^2-boundary the solutions of the Dirichlet problem (1.1) possess the following convergence property,

$$u^\varepsilon \rightharpoonup U \text{ in } \mathcal{W}, \text{ and } a^\varepsilon\nabla u^\varepsilon \rightharpoonup A\nabla U, \text{ in } (L^2((0,T)\times\Omega))^d, \text{ as } \varepsilon\to 0, \tag{2.1}$$

where U is the solution of the Dirichlet problem

$$\begin{aligned} U_t - \nabla\cdot(A(x)\nabla U) &= f(t,x), && \text{in } (0,T)\times\Omega,\\ U(0,x) &= u_0(x), && \text{in } \Omega,\\ U(t,x) &= g(t,x), && \text{on } (0,T)\times\partial\Omega. \end{aligned} \tag{2.2}$$

and $\mathcal{W} = \{v |\, v \in L^2(0,T;H_0^1(\Omega)),\ v' \in L^2(0,T;H^{-1}(\Omega))\}$. The homogenized matrix A is given by [6, 26]:

$$A(x) = \frac{1}{|Y|}\int_Y a(x,y)(I_d + \nabla_y \chi)dy, \tag{2.3}$$

where $\chi = (\chi_1, \cdots, \chi_d)$ is given by the solution of the cell problems

$$-\nabla_y \cdot (a(x,y)\nabla_y \chi) = \nabla_y \cdot a(x,y), \qquad y \in Y,$$

i.e.

$$-\sum_{i=1}^{d}\frac{\partial}{\partial y_i}(\sum_{k=1}^{d} a_{ik}\frac{\partial \chi_j}{\partial y_k}) = \sum_{i=1}^{d}\frac{\partial a_{ij}}{\partial y_i}, \quad j = 1, ..., d,$$

where also $\chi(x,y)$ is Y-periodic in y and $\int_Y \chi_j(x,y)dy = 0$.

2.2. **Inverse problem.** Let Ω be a bounded, open domain in $\mathbb{R}^d$, $d \geq 2$, of class $C^{1,1}$. In the classical theory of inverse problems, the following Dirichlet problem has been studied as a forward model

$$\begin{aligned} u_t - \nabla \cdot (A\nabla u) &= f(t,x), && \text{in } (0,T)\times\Omega, \\ u(x,0) &= u_0(x), && \text{in } \Omega, \\ u &= g, && \text{on } \partial\Omega. \end{aligned} \tag{2.4}$$

The coefficient A is, in general, a uniformly positive definite, symmetric, $d \times d$ matrix (it means, there exists a positive α such that for all X, $X^T AX \geq \alpha \|X\|^2$).

From the regularity theory we know that for $g \in H^{3/2}(\partial\Omega)$, this problem has a unique solution $u \in C^1\left([0,T];H^1(\Omega)\right) \cap C\left([0,T];H^2(\Omega)\right)$. We define the *Dirichlet-to-Neumann map* $\Lambda_A : C\left([0,T];H^{3/2}(\partial\Omega)\right) \to H^{1/2}(\partial\Omega)$ by

$$\Lambda_A(g) = A\nabla u \cdot n_{|\partial\Omega}. \tag{2.5}$$

The inverse problem is to determine the unknown diffusion coefficient $A(x)$ from the knowledge of the map Λ_A. To have the uniqueness of solution for the inverse problem, we consider $A(x)$ to have the form $A(x) = a(x)I_d$, where $a(x)$ is a scalar-valued function. In addition, we suppose the following regularity assumptions:

$$a \in W^{1,p}(\Omega), \text{ for some } p > 2, \text{ when } d = 2, \tag{2.6}$$

or

$$a \in C^{1,(1/2)+\zeta}(\bar{\Omega}), \text{ for some } \zeta > 0, \text{ when } d \geq 3. \tag{2.7}$$

Theorem 2.1. *(Theorem 1.3 in [13]) Let A_j for $j = 0, 1$ be two functions satisfying conditions (2.6) and (2.7). We denote by u_j the solution of problem (2.4) for $A = A_j$ and also let Λ_j be the corresponding Dirichlet-to-Neumann map. Suppose that*

$$\Lambda_0(g) = \Lambda_1(g), \qquad \text{in } H^{1/2}(\partial\Omega), \text{ for all } g \in C([0,T];H^{3/2}(\partial\Omega)). \tag{2.8}$$

Then $A_0 = A_1$ in Ω.

In this work we study the inverse problem with priori knowledge that diffusion term comes from (1.4). We assume that the Dirichlet-to-Neumann map, $\tilde{\Lambda}$ is known on a finite dimension subspace $G \subset C([0,T];H^{3/2}(\partial\Omega))$ and look for the parameter m that solves

$$\min_m \|\Lambda_{a^\varepsilon(m,\cdot)} - \tilde{\Lambda}\|, \qquad (IP^\varepsilon),$$

$\|.\|$ denotes the Frobenius norm. However, this problem is ill-posed and has a large computational cost [18]. To overcome this problem, we apply some multiscale methods to improve minimization functional (IP^ε). We replace the full inverse problem (IP^ε) with an effective inverse problem, that are based on ideas from homogenization theory, as follows

$$\min_m \|\Lambda_{A(m,\cdot)} - \tilde{\Lambda}\|, \qquad (IP_{Analytic}),$$

where $A(m,\cdot)$ is corresponding homogenized matrix which obtained by (2.3).

In [26], this idea has been followed for elliptic equation. Although this reduced formulation is often well-posed and results in a lower sensitivity to noise, this approach loses some details about microscale features.

It is noteworthy that homogenization convergence (2.1) yields the weak* convergence of Λ_{a^ε} to Λ_A in $H^{-1/2}(\partial\Omega)$. Indeed, for an arbitrary function $v \in H^1(\Omega)$ and $v|_{\partial\Omega} = h$ we have

$$\langle \Lambda_{a^\varepsilon}(g), h\rangle = \int_\Omega (u_t^\varepsilon v + a^\varepsilon \nabla u^\varepsilon \cdot \nabla v)dx, \tag{2.9}$$

where $\langle \cdot, \cdot \rangle$ is the duality pairing between $H^{-1/2}(\partial\Omega)$ and $H^{1/2}(\partial\Omega)$. Now if we apply (2.1), we will obtain

$$\langle \Lambda_{a^\varepsilon}(g), h\rangle \longrightarrow \langle \Lambda_A(g), h\rangle, \text{ for all } h \in H^{1/2}(\partial\Omega).$$

It makes sense, therefore, to consider the norm in problem $(IP_{Analytic})$ to be the norm of space $L(G, H^{-1/2}(\partial\Omega))$. Before going on, let us try to explain how we estimate $L(G, H^{-1/2}(\partial\Omega))$-norm. To apply Λ_A in (2.5), we need the derivative of u on $\partial\Omega$ which is not easy to provide, so we use (2.9) instead. Consider a finite dimensional subspace $H \subset H^{1/2}(\partial\Omega)$ and assume that $\{g_1, \cdots, g_L\}$ and $\{h_1, \cdots, h_J\}$ are bases of G and H, respectively. The matrix $[\tilde{\Lambda}_{ij}]$ represents the operator $\tilde{\Lambda}$, where $\tilde{\Lambda}_{ij} = \langle \tilde{\Lambda}(g_i), h_j\rangle$. Similarly, we may apply same representation for operators $\Lambda_{A(m,\cdot)}$ and $\Lambda_{a^\varepsilon(m,\cdot)}$ and then (IP^ε) or $(IP_{Analytic})$ will give a reasonable estimations for corresponding matrices.

3. FE-HMM

The explicit form of the homogenized coefficient is often unavailable, and therefore we cannot apply direct computation of macroscopic predictions. This challenge can be removed numerically with some multiscale methods, for this purpose we will introduce FH-HMM in this section and LOD method in the next. Heterogeneous multiscale method was first introduced by B. Engquist [17]. In this method a general macroscopic scheme on a macrogrid has been used to predict the missing macroscopic data from the microscopic model. The effectiveness of HMM is based on its ability to recover missing macroscale data from microscale models by applying the scale separation technique. Assume that $a^\varepsilon(x) = a(x, x/\varepsilon)$ is Y-periodic in second variable and admits scale separation between slow, x, and fast variables, x/ε. The aim of the Finite Element Heterogeneous Multiscale Method (FE-HMM) is to obtain the homogenized (coarse) solution U of (2.2) without directly computing $A(x)$ only by using input data in (1.1). Furthermore, when a sampling domain has been used, we do not need oscillatory data of (1.1) on the whole of computational domain. There are some applications of this approach, for instance, in material sciences problems, modern scanning and microscopy techniques we may only be able to acces to a local domain with fine scale structure, or in geosciences, we require some knowledge about a landscape, which might be sparsely available rather than a connected domain [7]. The macroscopic solver for (1.1) is the standard piecewise linear Finite Element Method over a macroscopic triangulation $\mathcal{T}_H$ with mesh size $H > \varepsilon$ and the time backward Euler scheme. We have the following macroscale weak form for the HMM [7, 25],

$$((U^n - U^{n-1})/\Delta t), V) + B(U^n, V) = (f^n, V) - B(g^n, V), \quad \text{for all } V \in X_H,$$

where U^n in the macroscopic Finite Element space X_H, is the solution of the problem, for $1 \le n \le N$, $t_n = n\Delta t$ with $\Delta t = T/N$, $f^n = \frac{1}{\Delta t}\int_{t_n}^{t_{n+1}} f(x,s)ds$ and g^n is Dirichlet boundary condition defined in the same way as f^n. Since we do not have the effective coefficient A_{HMM} explicitly, we evaluate the stiffness matrix

$$\begin{aligned} B(W,V) &= \int_\Omega \nabla W \cdot A_{HMM}(x)\nabla V dx = \sum_{K\in\mathcal{T}_H} \int_K \nabla W \cdot A_{HMM}(x)\nabla V dx \\ &\simeq \sum_{K\in\mathcal{T}_H} |K| \nabla W \cdot A_{HMM}(x_K)\nabla V, \qquad V, W \in X_H, \end{aligned} \tag{3.1}$$

where x_K is barycenter of K. Each entry of (3.1) is approximated by solving the following cell problem on subdomain $I_\delta(x_K) := x_K \pm \frac{\delta}{2} I$,

$$\begin{aligned} -\nabla \cdot (a^\varepsilon \nabla v^\varepsilon) &= 0, \qquad \text{in } I_\delta(x_K), \\ v^\varepsilon &= V, \qquad \text{on } \partial I_\delta(x_K). \end{aligned}$$

A standard Finite Element solver is utilized once more on a triangulation $\mathcal{T}_h$ of the subdomains. The spacing $h < \varepsilon$ is chosen sufficiently small in order to resolve the microscale. In the same way, w^ε is calculated as well and then we have

$$\nabla W \cdot A_{HMM}(x_K)\nabla V \simeq \frac{1}{|I_\delta|}\int_{I_\delta} \nabla w^\varepsilon \cdot a^\varepsilon \nabla v^\varepsilon dx.$$

Thus, we can rewrite

$$B(W,V) = \sum_{K\in\mathcal{T}_H} \frac{|K|}{|I_\delta|}\int_{I_\delta} \nabla w^\varepsilon \cdot a^\varepsilon \nabla v^\varepsilon dx.$$

$B(g^n, V)$ is also, evaluated in a same way. Figure 1 shows the macro-micro grid coupling in a typical FEM-HMM formulation.

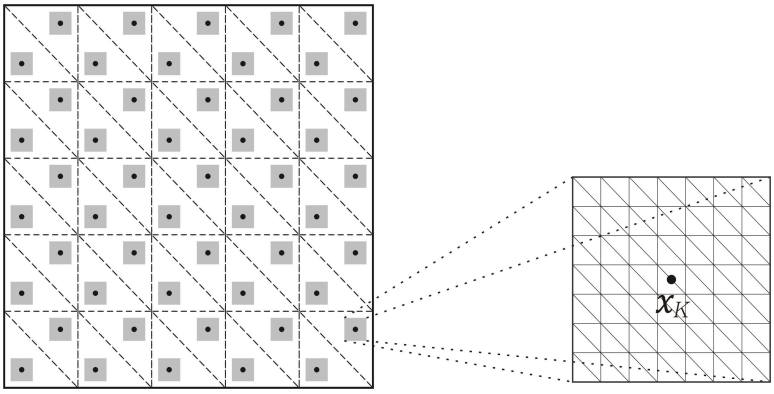

FIGURE 1. An illustration of macro-micro coupled grids used in FE-HMM.

Theorem 3.1. *(Theorem 1.1 in [25]) Let*

$$e(HMM) = \max_{x_K\in K, K\in\mathcal{T}_H} \|A(x_K) - A_{HMM}(x_K)\|,$$

where $\|\cdot\|$ denotes the Euclidean norm. Let U and U_{HMM} be the solution of (2.2) and FE-HMM, respectively. If U is sufficiently smooth, then there exists a constant C that is independent of $\varepsilon, \delta, H, \Delta t$, such that

$$\|U^N_{HMM} - U(\cdot,T)\|_{L^2(\Omega)} + \|U_{HMM} - U\|_* \le C(\Delta t + H^2 + e(HMM)),$$
$$\|U^N_{HMM} - U(\cdot,T)\|_{H^1(\Omega)} \le C(\Delta t + H + e(HMM)\Delta t^{-1/2}),$$

where $\|\cdot\|_*$ is the weighted space-time H^1 norm that is defined for every $V = \{V^n\}_{n=1}^N$ with $V^n \in X_H$ for $n = 1, ..., N$ as

$$\|V\|_* = (\sum_{n=1}^{N} \Delta t \|\nabla V^n\|_0^2)^{1/2}.$$

This result ensures that U^n_{HMM} converge to $U(\cdot, t_n)$ as $e(HMM)$ vanishes. This condition can be settled by corollary 1.4. Theorem 1.2 in [25] which states

$$e(HMM) \le C(\delta + \frac{\varepsilon}{\delta}).$$

It's remarkable that the bound for e(HMM) can be improved to fourth order in terms of ε/δ using the approach [19], second order in ε/δ using the approach of [12], and arbitrarily high order using [8, 9] and exponentially decaying using the approaches [1–3].

Remark 3.2. We denote the solution corresponding to $a^\varepsilon(m,x)$ by $U_{HMM}(m)$ for every parameter m. Also the estimate of the Dirichlet-to-Neumann map will be shown by $\Lambda_{HMM}(m)$. By this notation, the inverse problem $(IP_{Analytic})$ is formulated as

$$\min_m \|\Lambda_{HMM}(m) - \tilde{\Lambda}\|_{L(G,H^{-1/2}(\partial\Omega))}, \qquad (IP_{HMM}).$$

4. Localized Orthogonal Decomposition method

The Localized orthogonal Decomposition (LOD) method was first introduced by Målqvist and Peterseim in [23]. Classical homogenization theory is based on some structural assumptions on the diffusion coefficient, like periodicity and scale separation. This method decomposes the solution space into a finite dimensional (coarse) space and a residual space for the fine scales. In LOD method, the basis functions are constructed with diffusion coefficient information and have support on small vertex patches, [24]. In doing this, the assumption of periodicity of the microstructure is not needed.

Suppose $\mathcal{T}_H$ indicates a standard Finite Element mesh of Ω with the local mesh size $H_T := \text{diam(T)}$ for $T \in \mathcal{T}_H$ and a maximum mesh size of $H := \max_{T\in\mathcal{T}_H} H_T$. We assume that $\mathcal{T}_H$ is quasi-uniform, it means there exists a generic constant $\eta > 0$ such that

$$\min_{T\in\mathcal{T}_H} H_T > \eta H. \tag{4.1}$$

Now we define,

$$\sigma := \max_{T\in\mathcal{T}_H} \frac{H_T}{\text{diam}(B_T)} > 1, \tag{4.2}$$

where B_T is the largest ball contained in $T \in \mathcal{T}_H$. This constant is called the shape regularity and represents the quality of the mesh.

We need another scale $h < H$ that is small enough to resolve all related microscopic aspects of the problem to construct accurate discretization methods on the scale H. In this scale, the Finite Element mesh $\mathcal{T}_h$ is obtained from $\mathcal{T}_H$ using uniform refinement, for example, making 2^d finer meshes by halving the sides of the former meshes. This ensures that mesh uniformity and shape regularity are preserved in $\mathcal{T}_h$, while $\mathcal{T}_h$ is satisfied in (4.1) and (4.2) with the same constants. We shall also emphasize that the global mesh $\mathcal{T}_h$ is used theoretically, but, in practice, $\mathcal{T}_h$ will only be explored locally.

For $\mathcal{T} = \mathcal{T}_h, \mathcal{T}_H$, we denote

$$P^1(\mathcal{T}) := \{v : \Omega \to R \,|\, \forall T \in \mathcal{T}, v|_T \text{ is a polynomial of degree } 1\},$$

and define the spaces $V_H := P^1(\mathcal{T}_H)\cap H_0^1(\Omega)$ and $V_h := P^1(\mathcal{T}_h)\cap H_0^1(\Omega)$, so that $V_H \subseteq V_h$. Suppose $\mathcal{N}_H$ denotes the set of interior nodes of $\mathcal{T}_H$, and $\Pi_z \in V_H$ also denotes the corresponding nodal basis function (test/hat function) specified by the Lagrange property of its nodal values, $\Pi_z(z) = 1$ and $\Pi_z(y) = 0, \forall y \in \mathcal{N}_H \setminus \{z\}$, such that $\text{span}(\{\Pi_z\}_{z\in\mathcal{N}_H}) = V_H$.

For finding $U_n \in V_h$, we apply the notation $\bar{\partial}_t U = (U_n - U_{n-1})/\Delta t$ to the classical backward Euler FEM with uniform discretization in time,

$$(\bar{\partial}_t U, v) + b(U_n, v) = (f_n, v), \quad \forall\, v \in V_h, \tag{4.3}$$

for $n = 1, ...N$, $U_0 \in V_h$ is initial approximation of u_0 and $f_n := f(n\Delta t, \cdot)$, where, $b(u,v) = \int_\Omega a^\varepsilon \nabla u \cdot \nabla v dx$.

The aim of this method is to find an approximate solution, $\hat{U}_n$, in some subspace $\hat{V} \subset V_h$, such that dim $\hat{V}$ = dim V_H and the error $\|U_n - \hat{U}_n\| \le CH^2$ is valid. Here, the constant C is independent of the variations in a^ε, and $\hat{U}_n$ is less expensive than U_n to compute.

Now, a generalized Finite Element Method (GFEM) space is constructed by orthogonal decomposition using only the diffusion coefficient a^ε. It has been proven in [22] that this space is actually sufficient to achieve method convergence.

The (weighted) Clément interpolation operator $\mathcal{J}_H : V_h \to V_H$ is used to construct space $\hat{V}$ and defined by

$$\mathcal{J}_H v = \sum_{z \in \mathcal{N}_H} (\mathcal{J}_H v)(z)\Pi_z, \quad \text{where} \quad (\mathcal{J}_H v)(z) := \frac{\int_\Omega v\Pi_z dx}{\int_\Omega \Pi_z dx}. \tag{4.4}$$

Denote the kernel of the Clément interpolation operator (4.4) by $V^f = \{v \in V_h : \mathcal{J}_H v = 0\}$. This space contains all fine scale characteristics not achieving on V_H. Then, the space V_h can be decomposed into $V_h = V_H \oplus V^f$, in fact for each $v \in V_h$ we have $v = v_H + v^f$, where $v_H \in V_H$ and $v^f \in V^f$ and $(v_H, v^f) = 0$, where $(u, v) = \int_\Omega uvdx$ is the classical L_2 inner product.

We now define the orthogonal projection $R^f : V_h \to V^f$ as follows

$$b(R^f v, w) = b(v, w), \quad \forall\, w \in V^f,\ v \in V_h.$$

Accordingly the GFEM space, which is called the multiscale space, can be defined so that

$$V^{ms} := V_H - R^f V_H,$$

which leads to some other orthogonal decomposition $V_h = V^{ms} \oplus V^f$. We want to find the projection R^f of the nodal basis function $\Pi_x \in V_H$, for constructing a basis for V^{ms}. Let's call this projection $\mathcal{C}\Pi_x$, such that $\mathcal{C}\Pi_x \in V^f$ is a solution to the (global) corrector problem

$$b(\mathcal{C}\Pi_x, w) = b(\Pi_x, w), \quad \forall\, w \in V^f. \tag{4.5}$$

As a result, the multiscale space V^{ms} has a basis that is given by $\{\Pi_x - \mathcal{C}\Pi_x : x \in \mathcal{N}_H\}$. Furthermore, we also define the projection $R^{ms} : V_h \to V^{ms}$, by

$$b(R^{ms} v, w) = b(v, w), \quad \forall\, w \in V^{ms},\ v \in V_h.$$

Note that $R^{ms} = I - R^f$. Now define the corresponding GFEM to (4.3) to find $U_n^{ms} \in V^{ms}$ such that

$$\begin{aligned} (\bar{\partial}_t U_n^{ms}, v) + b(U_n^{ms}, v) &= (f_n, v), \quad \forall\, v \in V^{ms}, \\ (U_0^{ms}, v) &= (U_0, v), \quad \forall\, v \in V^{ms}, \end{aligned} \tag{4.6}$$

for $n = 1, ..., N$. Solving the corrector problems (4.5) is computationally costly because they are posed in the fine scale space V^f. Furthermore, since the correctors $\mathcal{C}\Pi_x$ have global support in general, the resulting linear system (4.6) is damaged in the sense of sparsity. However, according to [23], $\mathcal{C}\Pi_x$ decays exponentially. This experiment leads to localize the corrector problems to smaller patches of coarse elements as a result of the observation. We employ a variation described in [22], which decreases the needed patch size. A patch with size k for every $K \in \mathcal{T}_H$, $\omega_k(K)$, is defined as

$$\omega_0(K) := \operatorname{int} K,$$

$$\omega_k(K) := \operatorname{int}\left(\cup\{\hat{K} \in \mathcal{T}_H : \hat{K} \cap \overline{\omega_{k-1}(K)} \neq \emptyset\}\right), \quad k = 1, 2, \ldots .$$

Figure 2 illustrates how patches enlarge as k increases. It is also noted that, $V^f(\omega_k(K)) := \{\omega \in V^f : v(z) = 0 \text{ on } \bar{\Omega} \setminus \omega_k(K)\}$. Define $R_K^f : V_h \to V^f$,

$$\int_\Omega a^\varepsilon(x)\nabla(R_K^f v)\cdot\nabla w = \int_K a^\varepsilon(x)\nabla v\cdot\nabla w, \qquad \forall\, v \in V_h,\ w \in V^f,$$

also it is remarked that $R^f := \sum_{K\in\mathcal{T}_H} R_K^f$. The operator $R_{K,k}^f : V_h \to V^f(\omega_k(K))$ is a localization of R_K^f,

$$\int_{\omega_k(K)} a^\varepsilon(x)\nabla(R_{K,k}^f v)\cdot\nabla w = \int_K a^\varepsilon(x)\nabla v\cdot\nabla w, \qquad \forall\, v \in V_h,\ w \in \omega_k(K),$$

Regarding $R_k^f := \sum_{K\in\mathcal{T}_H} R_{K,k}^f$, we introduce a localized multiscale space for each nonnegative integer k as, $V_k^{ms} := V_H - R_k^f V_H$. Indeed, $\{\Pi_x - \mathcal{C}^k\Pi_x : x \in \mathcal{N}_H\}$ is a basis for V_k^{ms}, where $\mathcal{C}^k\Pi_x = R_k^f\Pi_x$ is the localized version of $\mathcal{C}\Pi_x$. The *local orthogonal decomposition* refers to the process of decomposing V_h into the orthogonal spaces V^{ms} and V^f, which V_k^{ms} is the localized version of V^{ms}.

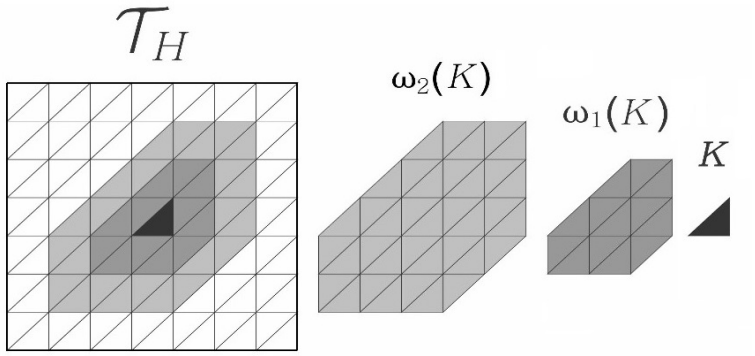

FIGURE 2. Illustration of patches around an element K.

Lemma 4.1. *(Lemma 3.4 in [22]) Suppose α and β are constants defined in (1.2). Then there exist a constant $0 < \mu < 1$ that depends on the contrast β/α such that*

$$\|R^f v - R_k^f v\|_+ \leq C k^{d/2} \mu^k \|v\|_+, \quad v \in V_h,$$

where C depends on α, β and σ, but not on the variations of a^ε and $\|\cdot\|_+ := \|(a^\varepsilon)^{1/2}\nabla \cdot \|$.

The orthogonal projection $R_k^{ms} : V_h \to V_k^{ms}$ is defined by

$$b(R_k^{ms} v, w) = b(v, w), \quad \forall\, w \in V_k^{ms},$$

and we replace V^{ms} by V_k^{ms} to have the localization of (4.6). The purpose of localized GFEM formulation is to find $U_{k,n}^{ms} \in V_k^{ms}$ such that

$$\begin{aligned} (\bar{\partial}_t U_{k,n}^{ms}, v) + b(U_{k,n}^{ms}, v) &= (f_n, v), \qquad \forall\, v \in V_k^{ms}, \\ (U_{k,0}^{ms}, v) &= (U_0, v), \qquad \forall\, v \in V_k^{ms}, \end{aligned} \tag{4.7}$$

for $n = 1, ..., N$.

Theorem 4.2. *(Theorem 4.1 in [22]) Let U_n be the solution to (4.3) and $U_{k,n}^{ms}$ the solution to (4.7). Then, for $1 \leq n \leq N$,*

$$\|U_{k,n}^{ms} - U_n\|_{L^2(\Omega)} \leq C(1 + \log \frac{t_n}{\Delta t})(H + k^{d/2}\mu^k)^2 (t_n^{-1}\|U_0\|_{L^2(\Omega)} + \|f\|_{L_\infty(0,T,L_2(\Omega))} + \|\dot{f}\|_{L_\infty(0,T,L_2(\Omega))}),$$

where C depends on α, β and σ; and t_N is final time.

Remark 4.3. (Remark 4.6 in [22]) We note that the choice of k and the size of μ determine the rate of the convergence. In general, to achieve optimal order convergence rate, k should be chosen proportional to the $\log(H^{-1})$, i.e. $k = c\log(H^{-1})$. With this choice of k we have $\|U_{k,n}^{ms} - U_n\|_{L^2(\Omega)} \leq C(1 + \log n)H^2\, t_n^{-1}$.

If we have inhomogeneous boundary condition in (1.1), we will introduce Sobolev space

$$V := H_{0,\partial\Omega}^1(\Omega) = \{v \in\ H^1(\Omega)\ : v|_{\partial\Omega} = 0\},$$

and let $U = \hat{U} + g$ with $\hat{U} \in V$. In this case the full approximation is

$$U_H^{ms} := \hat{U}_H^{ms} + \omega_g + g,$$

where

$$b(\hat{U}_H^{ms},\ v) = \int_\Omega f v dx\ -\ b(g, v),$$

and

$$b(\omega_g,\ v) = -a(g, v),\ \text{for all}\ \ v \in W,$$

W is fine scale space [24].

Let Ω be the unit square, $f(x,t) = 0$, $u_0 = 1$ and $u|_{\partial\Omega} = tx^2$. Our reference mesh size is $h = 2^8$ and the variation range of H is $H = 2^2, 2^3, 2^{3.5}, 2^4, 2^{4.5}, 2^5$.

The backward Euler LOD approach is compared to the standard backward Euler Finite Element Method. We compare the error in the L^2-norm between these solutions and the reference solutions at final time $T = 1$ vs. H. The time step is $\Delta t = 0.01$. Refer to Figure 3 for the LOD method, we observe optimal convergence.

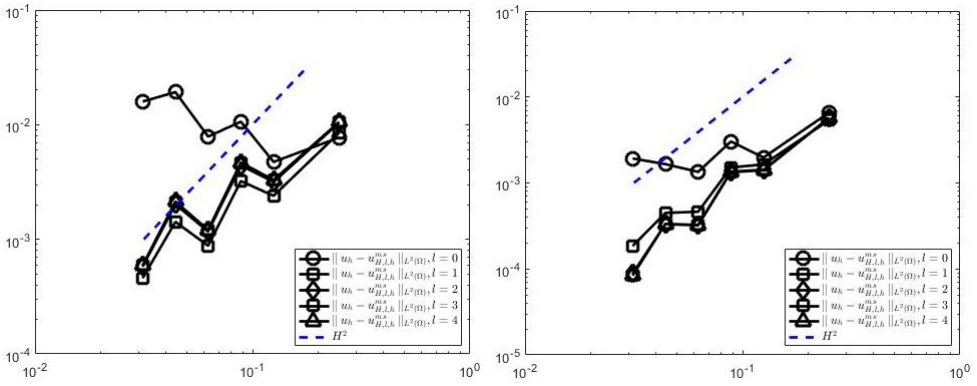

FIGURE 3. Error in $L^2 - norm$ vs. H. Left: periodic diffusion coefficient as Model A (5.1), Right: Nonperiodic diffusion coefficient as Model B (5.2).

Remark 4.4. We denote the solution corresponding to $a^\varepsilon(m,x)$by $U_{LOD}(m)$ for every parameter m. Also the estimate of the Dirichlet-to-Neumann map will be shown by $\Lambda_{LOD}(m)$. By this notation, the inverse problem (IP_{LOD}) is formulated as

$$\min_m \|\Lambda_{LOD}(m) - \tilde{\Lambda}\|_{L(G,H^{-1/2}(\partial\Omega))}, \qquad (IP_{LOD}).$$

5. Numerical experiments

This section is devoted to provide some examples of numerical experiments to illustrate the behavior of the proposed numerical methods for solving the inverse problems.

First, we emphasize that solving the full problem (1.1) on a fine mesh $\mathcal{T}_h$ with resolution $h < \varepsilon$, simulates the observational data, $\tilde{\Lambda}$ for some $\tilde{m}$. Here, we estimate the Dirichlet-to-Neumann map in finite space $L(G,H)$ as we discussed in Section 2, in which G and H have basis $G = \{x, y, x^2, y^2, xy, t, xt, yt, x^2t, y^2t, xyt\}$ and $H = \{x, y, x^2, y^2, xy\}$. As a result, we are able to recover the parameter m by solving problems $(IP_{Analytic})$, (IP_{HMM}) and (IP_{LOD}) separately. Table 1 illustrates how we recovered the parameter m and what the relative errors $\frac{|m-\tilde{m}|}{|\tilde{m}|}$ are.

In all of the simulations, a standard $\mathcal{P}^1$ Finite Element Method is used on a regular triangulation of the domain. In our examples we use the microsoft.matlab.2020 package on a computer equipped with the following specifications: Windows 10 Pro with 64-bit operating system, 32 GB of RAM, and Intel Core i7-9700 processor. Minimization is performed using the MATLAB fminbnd function. The implementation of the LOD method using MATLAB code in Chapter 7 of [24] is done. We set $\Omega = [0,1] \times [0,1]$, $\varepsilon = 1/100$, $H = 1/16$, $h = 1/256$, $T_0 = 1$, $\Delta t = 0.01$, $f = 0$, $\delta = \varepsilon$ for HMM, and $l = 2$ for LOD method.

Example 5.1. *Model A.* The microstructure model is represented by the multiscale function

$$a^{\varepsilon}(m,x) = 1.1 + m\sin(2\pi x_2/\varepsilon), \tag{5.1}$$

The coefficient a^{ε} is plotted in the left side of Figure 4. The corresponding homogenized coefficient is [18]

$$A(m) = \begin{pmatrix} \langle a(m,\cdot)\rangle & 0 \\ 0 & \langle a(m,\cdot)^{-1}\rangle^{-1} \end{pmatrix},$$

where $\langle a(m,\cdot)\rangle = \frac{1}{|\Omega|}\int_{\Omega} a(m,x)dx$.

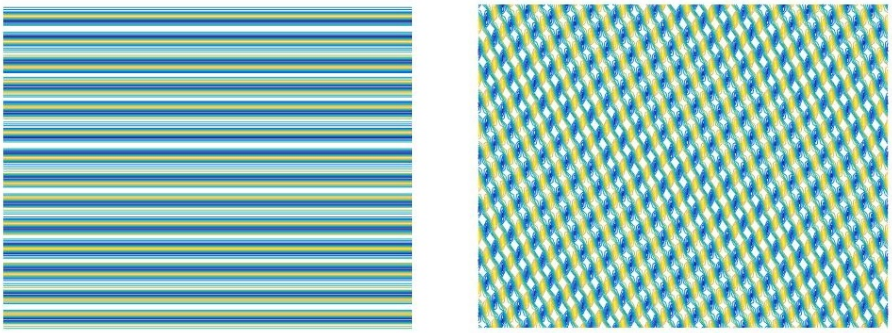

FIGURE 4. Left: Model A, Right: Model B.

Example 5.2. *Model B.* Here, the microstructure model is of the form of the following multiscale function

$$a^{\varepsilon}(m,x) = 1.1 + \sin(2\pi\hat{x}_2/\varepsilon), \quad \hat{x} = \varrho_m x,$$

such that

$$\varrho_m = \begin{pmatrix} \cos(2\pi m) & \sin(2\pi m) \\ -\sin(2\pi m) & \cos(2\pi m) \end{pmatrix},$$

This coefficient a^{ε} is also plotted in the right side of Figure 4 and the corresponding homogenized coefficient is [18]

$$A(m) = \varrho_m^T \begin{pmatrix} \langle a(m,.)\rangle & 0 \\ 0 & \langle a(m,.)^{-1}\rangle^{-1} \end{pmatrix} \varrho_m.$$

Example 5.3. *Model C.* The analog of Model A is a class of separable functions a^{ε}, The microstructure model is represented by the multiscale function

$$a^{\varepsilon}(m,y) = a_1^{\varepsilon}(m,y_1)a_2^{\varepsilon}(m,y_2),$$

where a_1^{ε} and a_2^{ε} of the type in (5.1) (see Figure 5). According to [18], the corresponding homogenized coefficient is

$$A(m) = \begin{pmatrix} \langle a_1(m,.)^{-1}\rangle^{-1}\langle a_2(m,.)\rangle & 0 \\ 0 & \langle a_2(m,.)^{-1}\rangle^{-1}\langle a_1(m,.)\rangle \end{pmatrix}.$$

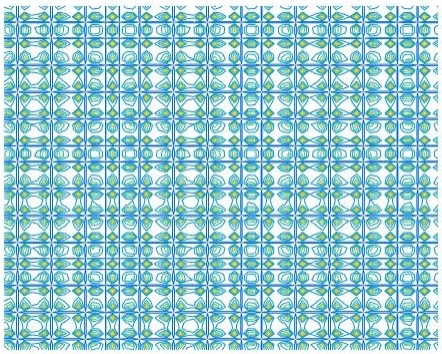

FIGURE 5. Model C.

Example 5.4. *Model D.* The microstructure model is represented by the multiscale function

$$a^{\varepsilon}(m,x) = \frac{(R_1 + m\,\sin(2\pi x_1)) + (R_1 + m\,\cos(2\pi x_2))}{(R_1 + m\,\sin(2\pi x_1/\varepsilon))(R_1 + m\,\sin(2\pi x_2/\varepsilon))} I,$$

Figure 6 depicts the coefficient a^{ε} [16].

$$A(m,x) = \frac{(R_1 + m\,\sin(2\pi x_1)) + (R_1 + m\,\cos(2\pi x_2))}{R_1\sqrt{R_1^2 - m^2}} I.$$

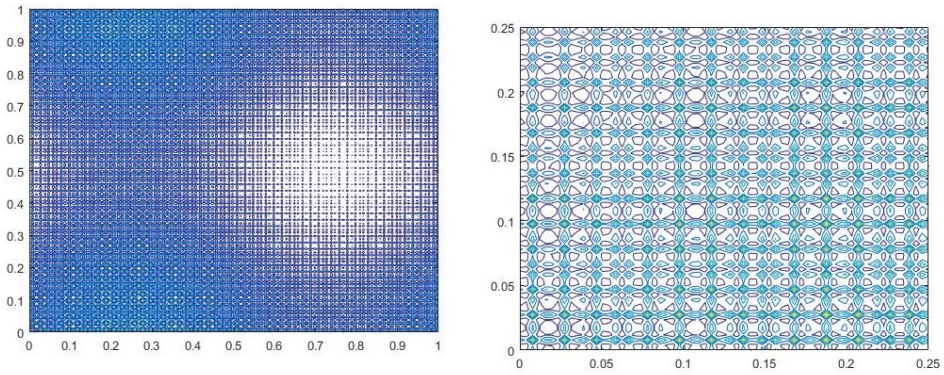

FIGURE 6. Model D. Left: Macroscale, Right: Microscale.

Table 1 shows the relative error in the estimation of the microscale parameter $m \in \mathbb{R}$. Our experiments for finding relative errors show that the HMM and LOD are independent of choosing intervals. Table 2 contains a comparison of the performance time (in seconds) using different forward solvers. The differences in the inversion results can be attributed to the resolution of the meshes used, the mismatch between the oscillatory data and the slowly varying predictions, and errors caused by using the optimization routine.

TABLE 1. Relative error in inversion for a microscale parameter.

	Analytic	HMM	LOD
Model A	0.2633	0.0968	0.0098
Model B	0.0319	0.0318	1.3451e-05
Model C	0.0494	0.0469	0.2681
Model D	0.0273	0.1854	0.0029

TABLE 2. Time of inversion for a microscale parameter.

	Analytic	HMM	LOD
Model A	6	366	7835
Model B	0.3	299	5919
Model C	6	215	7872
Model D	7	412	9612

For the next examples, forward computations are made by LOD solver for macroscopic predictions. The results in Table 3 show the inversion results. Here we set $\varepsilon = 1/8$.

Example 5.5. *Nonperiodic Model.* Now, we consider the multiscale model, represented by the function

$$a^{\varepsilon}(m,x) = (2 - m\,\sin(2\pi\tan(\frac{15\pi}{32}x_1/\varepsilon))). \tag{5.2}$$

It is plotted in left side of Figure 7. Even though the periodicity is 15/4, it does not possess a periodic microstructure.

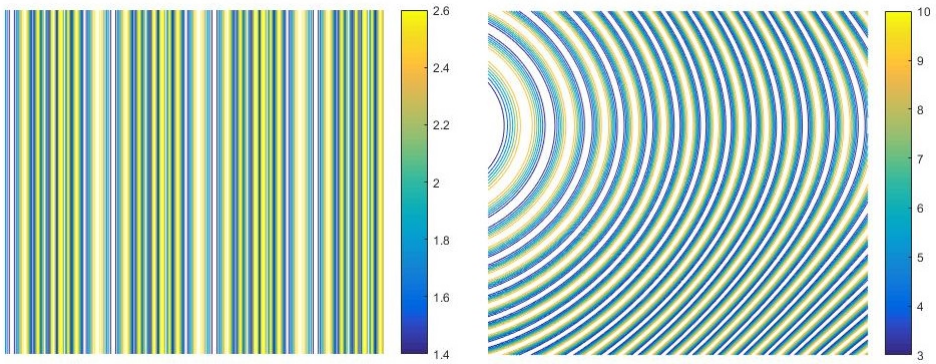

FIGURE 7. Left: Nonperiodic model, Right: Nonaffine model.

Example 5.6. *Nonaffine parameterized Model.*

Above Figures 4, 5, 6, and 7 demonstrate the contours of the diffusion coefficients with high oscillations in microscale, furthermore the Figure 6 depicts the difference of the oscillations in macro and micro scales.

We consider a nonaffine parametrization of the multiscale tensor. In this case the function $\varrho(m,x)$ controls the orientation of the oscillations of the full tensor $a^{\varepsilon}(m,x)$, which is defined as

$$a^{\varepsilon}(m,x) = 4(\cos(\frac{2\pi e^{1^T}Q}{\varepsilon}) + 1.5),$$

TABLE 3. Relative error for nonperiodic and nonaffine model.

Nonperiodic Model	0.0278
Nonaffine Model	2.2995e-04

TABLE 4. Microscale parameter inversion for a random microstructure. The true parameter is $\bar{m} = .6$ and the percentage of the recovered parameter m, lying in the given interval $I_{\bar{m}}$, is shown.

$I_{\bar{m}}$	l=1	l=2	l=3	l=4
[.5,.7]	58%	55%	63%	61%
[.55,.65]	11%	12%	15%	19%
[.59,.61]	7%	6%	6%	6%

where,

$$Q = \begin{pmatrix} \cos(2\pi\varrho(m,x_1)) & \sin(2\pi\varrho(m,x_2)) \\ -\sin(2\pi\varrho(m,x_1)) & \cos(2\pi\varrho(m,x_2)) \end{pmatrix}, \quad \varrho(m,x) = 1.05 + mx.$$

See right side of Figure 7.

Example 5.7. *Random microstructure* [24]. It is a model in which the microstructure is created by randomly selecting either a value $\beta = 1$ (black) or a value $\alpha = 1/100$ (white) with equal probability $1/2$ in each field of a Cartesian mesh of width $1/2^5$ multiplied by an unknown parameter m (Figure 8). These experiments involve the fixing of $\bar{m}$, and solving the minimization problem IP_{LOD}. It has been carried out for 100 realizations of $a^\varepsilon(m)$. We compare the performance of LOD forward solvers corresponding to four different choices of the size of the patches, $l = 1, 2, 3, 4$. The other parametrers are chosen $h = 1/2^7$ and $H = 1/2^3$. As seen in Table 4 the frequency of recovered parameters m that lie in the interval $I_{\bar{m}}$, centered at the true parameter and for different value of l, we have good results, and this is one of the advantages of the LOD method.

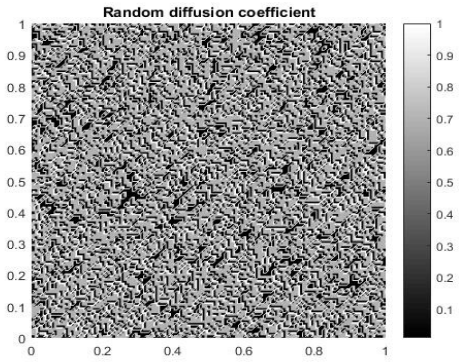

FIGURE 8. An example of randomly non-periodic diffusion coefficient.

6. CONCLUSION

We present computational techniques for solving inverse problems for multiscale parabolic partial differential equation. Instead of directly working with the effective equation we constrain the search space by representing the microscale

by a parameter in order to have a well-posed inverse problem. When the explicit form of the effective equation exists we use this form, otherwise, some numerical multiscale methods such as HMM and LOD method must be used. It is noted that in using LOD method, the diffusion coefficient dose not need to have some properties such as scale seperation, or periodicity and only belonging to L^∞ is sufficient. Here we presented 7 numerical examples which show the algorithm is convergent (using Frobenius-norm).The performance of this technique applied to random media is demonstrated (Example 5.7). Our experiments show that the LOD method is more precisely rather than other two, however the elapsed time using in this method is more than others, in other words the LOD method does not exploit the scale separation in comparison to HMM that becomes computationally more expensive when applied to problems with scale separation[3, 20].

Conflict of Interest and Acknowledgment

The authors declare that we have no conflict of interest. Data sharing not applicable to this article as no datasets were generated or analyzed during the current study. This is a joint-authored original work that has not been supported financially by any organizations. We are also extremely grateful to the esteemed officials of the journal of *Computational Methods for Differential Equations*" who precisely reviewed this article and gave constructive and useful instructions, we also applied all of them to enrich our article.

References

[1] A. Abdulle, D. Arjmand, and E. Paganoni, *Exponential decay of the resonance error in numerical homogenization via parabolic and elliptic cell problems*, C. R. Math. Acad. Sci. Paris, *357* (2019), 545–551.
[2] A. Abdulle, D. Arjmand, and E. Paganoni, *A parabolic local problem with exponential decay of the resonance error for numerical homogenization*, Mathematical Models and Methods in Applied Sciences, *31*(13) (2021), 2733–2772.
[3] A. Abdulle, D. Arjmand, and E. Paganoni, *An elliptic local problem with exponential decay of the resonance error for numerical homogenization*, Multiscale Modeling & Simulation, *21*(2) (2023), 513–541.
[4] A. Abdulle and A. Blasio, *A Bayesian Numerical Homogenization Method for Elliptic Multiscale Inverse Problems*, SIAM/ASA J. Uncertain. Quantif., *8* (2020), 414–450.
[5] A. Abdulle and A. Di Blasio, *Numerical homogenization and model order reduction for multiscale inverse problems*, Multiscale Model. Simul., *17* (2019), 399–433.
[6] A. Abdulle and W. E, *Finite difference heterogeneous multi-scale method for homogenization problems*, J. Comput. Phys., *191* (2003), 18– 39.
[7] A. Abdulle and A. Nonnenmacher, *A short and versatile finite element multiscale code for homogenization problems*, Comput. Methods Appl. Mech. Engrg., *198* (2009), 2839–2859.
[8] D. Arjmand and O. Runborg, *A time dependent approach for removing the cell boundary error in elliptic homogenization problems*, Journal of Computational Physics, *314*(2) (2016), 206–227.
[9] D. Arjmand and O. Runborg, *Estimates for the upscaling error in heterogeneous multiscale methods for wave propagation problems in locally periodic media*, Multiscale Modeling & Simulation, *15*(2) (2017), 948–976.
[10] L. Beilina, *Inverse problems and applications*, 2015.
[11] A. Bensoussan, J. L. Lions, and G. Papanicolaou, *Finite Asymptotic Analysis for Periodic Structures*, North-Holland, Amsterdam, 1978.
[12] X. Blanc and C. Le Bris, *Improving on computation of homogenized coefficients in the periodic and quasi-periodic settings*, Netw. Heterog. Media, *5*(1) (2010), 1–29.
[13] B. Canuto and O. Kavian, *Determining coefficients in a class of heat equations via boundary measurements*, SIAM J. Math. Anal., *32* (2001), 963–986.
[14] D. Cioranescu and P. Donato, *An Introduction to Homogenization*, Oxford University Press, Oxford, 1999.
[15] D. Colton, H. Engl, A. K. Louis, J. McLaughin, and W. Rundell, *Surveys on Solution, Methods for Inverse Problems*, Springer-Verlag, Wien, 2000.
[16] R. Du and P. Ming, *Heterogeneous multiscale finite element method with novel numerical integration schemes*, COMMUN. MATH. SCI., *8* (2010), 863–885.
[17] B. Engquist, *The heterogeneous multi-scale methods*, Commun. Math. Sci., *1* (2003), 87–132.

[18] C. Frederick and B. Engquist, *Numerical methods for multiscale inverse problems*, Commun. Math. Sci., *15*(2) (2017), 305–328.
[19] A. Gloria, *Reduction of the resonance error. Part 1: Approximation of homogenized coefficients*, Math. Models Methods Appl. Sci., *21*(8) (2011), 1601–1630.
[20] O. Jecker, *Optimization based methods for highly heterogeneous multiscale problems and multiscale methods for elastic waves*, No. 7467. EPFL, 2017.
[21] P. Ljung, R. Maier, and A. Maalqvist, *A space-time multiscale method for parabolic problems*, Multiscale Modeling & Simulation, *20*(2) (2022), 714–740.
[22] A. Maalqvist and A. Persson, *Multiscale techniques for parabolic equations*, Numer. Math., *138*(1) (2018), 191–217.
[23] A. Maalqvist and D. Peterseim, *Localization of elliptic multiscale problems*, Math. Comp., *83*(290) (2014), 2583–2603.
[24] A. Maalqvist and D. Peterseim, *Numerical homogenization by localized orthogonal decomposition*, Vol. 5 of SIAM Spotlights, Society for Industrial and Applied Mathematics (SIAM), Philadelphia, PA, 2020.
[25] P. Ming and P. Zhang, *Analysis of the heterogeneous multiscale method for parabolic homogenization problems*, J. AMS, *18*(1) (2006), 121– 156.
[26] J. Nolen, G. A. Pavliotis, and A. M. Stuart, *Multiscale Modelling and Inverse Problems*, Inverse Problems, Springer, *18*(1) (2010), 1– 32.